

PCCP

Accepted Manuscript



This is an *Accepted Manuscript*, which has been through the Royal Society of Chemistry peer review process and has been accepted for publication.

Accepted Manuscripts are published online shortly after acceptance, before technical editing, formatting and proof reading. Using this free service, authors can make their results available to the community, in citable form, before we publish the edited article. We will replace this *Accepted Manuscript* with the edited and formatted *Advance Article* as soon as it is available.

You can find more information about *Accepted Manuscripts* in the [Information for Authors](#).

Please note that technical editing may introduce minor changes to the text and/or graphics, which may alter content. The journal's standard [Terms & Conditions](#) and the [Ethical guidelines](#) still apply. In no event shall the Royal Society of Chemistry be held responsible for any errors or omissions in this *Accepted Manuscript* or any consequences arising from the use of any information it contains.



Physical Chemistry Chemical Physics

ARTICLE

Synthesis of α -MnO₂ nanowires modified by Co₃O₄ nanoparticles as a high-performance catalyst for rechargeable Li-O₂ batteries

Fan Wang,^a Zhaoyin Wen^{*a}, Chen Shen^a, Xiangwei Wu^a and Jianjun Liu^b

Received 00th January 20xx,
Accepted 00th January 20xx

DOI: 10.1039/x0xx00000x

www.rsc.org/

The α -MnO₂ nanowires uniformly coated with Co₃O₄ nanoparticles were prepared as a bi-functional catalyst for rechargeable Li-O₂ batteries. The α -MnO₂ nanowires were 5–20 nm in diameter, ranging between 5 and 10 μ m in length. And the coated Co₃O₄ nanoparticles were around 5 nm in diameter. The α -MnO₂/Co₃O₄ hybrid had a high specific surface area of 329.5 cm²·g⁻¹, and showed excellent catalytic property. Both of the charge and discharge overpotentials are effectively reduced and the batteries could stably work for more than 60 cycles. It is demonstrated that the catalytic performance of the α -MnO₂/Co₃O₄ hybrid is not only associated with the morphology and size of the catalyst, but also with their synergetic effects and the oxygen vacancies produced at the surface of MnO₂. The results of charge-discharge cycling tests demonstrate that this α -MnO₂/Co₃O₄ hybrid catalyst is a promising candidate for the Li-O₂ batteries.

Introduction

Recently, Li-O₂ batteries have gained worldwide attention due to the largest theoretical specific energy density (11972 Wh·kg⁻¹) among all the energy storage devices.^{1–3} The reaction in Li-O₂ batteries is based on the catalytic reaction other than the well-known intercalation reaction in typical lithium ion batteries.⁴ Moreover, during the cycle process, reactant oxygen is obtained directly from the environment rather than storing in inside the cell. This reaction mechanism determines Li-O₂ batteries a 10-fold higher energy density than conventional Li-ion batteries. Therefore, Li-O₂ batteries have gained recognition as one of the most attractive candidates to replace now widely used conventional Li-ion batteries.

Despite their appealing potential, there are several significant technical challenges remained with Li-O₂ batteries.⁵ Some critical challenges limiting the practical use of this technology include sluggish oxygen reduction reaction (ORR), low oxygen evolution reaction (OER) kinetics, low electron conductivity of the insulating discharge product Li₂O₂. These issues should be solved for their practical application. Many studies have thus focused on developing highly efficient catalysts for the air cathode in order to significantly improve the reaction kinetics.⁶ In previous efforts, many types of catalysts, such as noble metals, transition metal oxides, carbon based materials, transition-metal carbide have been used as catalysts to reduce the overpotential and enhance the cycling performance.^{7–15}

Up to now, MnO₂ and Co₃O₄ as low-cost and environmental friendly transition metal oxides have been applied as promising catalysts in Li-O₂ batteries. MnO₂ hollow spheres¹⁶, MnO₂ nanoflakes¹⁷, MnO₂ nanorods¹⁸, MnO₂ nanowires¹⁹ have been studied. The advantages of MnO₂ may be attributed to the high surface area which could deliver a high capacity²⁰ and good catalytic performance for OER and ORR.^{7, 21} Comparing to MnO₂, Co₃O₄ contain a higher electron conductivity. Free-standing Co₃O₄ nanorods²², mesoporous Co₃O₄²³, flowerlike Co₃O₄²⁴, etc. have been studied in Li-O₂ batteries. Those diverse morphologies showed different catalytic activity.

In order to further improve the ability of the catalysts for OER and ORR, hybrid catalysts such as MnO₂/CNT²⁵, MnO₂/GN¹⁸, Co₃O₄/RuO₂²⁶, etc. have also been prepared and used in Li-O₂ batteries. But the performance of those catalysts still is not satisfying. Compound with noble metals such as MnO₂/Pd²⁷, Pt/Co₃O₄²⁸ could largely reduce the charge potential, but with low capacity and high price.

Therefore, the design of a low-cost and stable bi-functional electrocatalyst is a major challenge to the construction of efficient Li-O₂ batteries. Transition metal oxides are promising catalysts for ORR and OER processes because of their low cost and environmental friendly.⁷ From the current reports, transition metal oxides hybrids have not drawn much attention. Few researches have been done about those catalysts in Li-O₂ batteries. MnO₂ is one kind of catalysts which has been widely used in Li-O₂ batteries. Due to its easy formation of high specific surface area nanostructure, the discharge products would have more deposition area, hence high specific capacity could be achieved. Theoretical calculation indicate that, good ORR catalytic performance of α -MnO₂ results from the facile oxygen vacancies formation at its surface.²⁹ Cobaltic oxide (Co₃O₄) as another kind of catalysts has low resistivity and high OER

^a CAS Key Laboratory of Materials for Energy Conversion, Shanghai Institute of Ceramics, Chinese Academy of Sciences, 1295 Ding Xi Road, Shanghai 200050, People's Republic of China. Email: zywen@mail.sic.ac.cn

^b State Key Laboratory of High Performance Ceramics and Superfine Microstructures, Shanghai Institute of Ceramics, Chinese Academy of Sciences, Shanghai 200050, People's Republic of China.

catalytic activity which can reduce the charge potential effectively. Combining these two kinds of catalysts to produce hybrid catalyst with the interaction and coping effects produced oxygen vacancies which could achieve promoted performance both for OER and ORR in Li-O₂ batteries.

In this report, we prepared a kind of high surface area α -MnO₂/Co₃O₄ nanomaterials as a bi-functional catalyst for rechargeable Li-O₂ batteries. The Co₃O₄ nanoparticles homogeneously coated on the α -MnO₂ nanowires which was considered to benefit the charge transfer without affecting the high surface area. With the synergistic effect and the interfacial effect between the α -MnO₂ nanowire and the Co₃O₄ nanoparticles which lead to the formation of oxygen vacancies on the surface of MnO₂, such a well-designed composite structure showed the improvement on both ORR and OER. The cycle performance was also greatly improved. More than 60 cycles were achieved with the capacity maintaining at 1000 mAh·g⁻¹. It is demonstrated that the α -MnO₂/Co₃O₄ hybrid could be promising catalysts in Li-O₂ batteries.

Experimental

1. Synthesis of α -MnO₂ Nanowires

The MnO₂ nanowires were synthesized by a hydrothermal method somewhat similar to a previous research.³⁰ In a typical procedure, 8 mmol analytical grade hydrate MnSO₄·H₂O and an equal amount of (NH₄)₂S₂O₈ were dissolved in 32 mL deionized water at room temperature. Then 20 mmol of (NH₄)₂SO₄ was added under vigorous stirring to form a clear solution. Finally, the mixture was transferred into a 40 mL Teflon-lined autoclave, heated for 12 hours at 140 °C in an air-flow oven. After it naturally cooled to room temperature, the dark brown product was collected by filtration and washed with deionized water, ethanol several times to remove impurities possibly remaining in the final products. The sample was obtained after finally drying at 80 °C for 10 hours in vacuum oven.

2. Synthesis of α -MnO₂/Co₃O₄ hybrid

87 mg as-prepared α -MnO₂ nanowires were dispersed in 35 mL deionized water by ultrasonic vibration for over 30 min to prepare a homogeneous suspension. 1mmol Co(NO₃)₂·6H₂O was added into the above suspension and the mixed solution was stirred for another 30 min. Then adjusted pH of the solution to 11 with ammonia. After that, the mixed solution was transferred to a 50 mL Teflon-lined stainless steel autoclave. The autoclave was sealed and maintained at 150°C for 10 hours. The products were collected by filtration and washed with deionized water and ethanol. The α -MnO₂/Co₃O₄ samples were obtained after finally dried at 80°C for 12 hours.

3. Li-O₂ Cell Assembly and Tests

The air cathodes were formed by mixing the catalyst of α -MnO₂/Co₃O₄, Ketjen black carbon (KB) and PVDF in NMP (with a weight ratio of 6:3:1), and evenly coated onto a nickel foam. An air electrode containing α -MnO₂ nanowires, Co₃O₄ nanoparticles, and α -MnO₂ mixed with Co₃O₄ nanoparticles

electrodes were also prepared respectively for comparison. The as-prepared electrodes were dried in vacuum oven at 80 °C for 24 hours. All electrodes loaded the similar material of about 0.8 mg·cm⁻². The cells used in this experiment were based on a Swagelok Cell design composed of a Li metal anode, an electrolyte of LiTFSI in TEGDME, a separator of Celgard 2400, and the as-prepared porous cathode. The galvanostatic charge and discharge tests were measured on a LAND CT2001A battery test system at ambient temperature after an 5 h rest period. All the specific capacities are calculated based on the mass of catalyst in the air electrodes.

4. Characterization

The products and electrode were characterized with a variety of analytical techniques. The crystal structure and phase were characterized by X-ray diffraction (XRD, Rigaku Ultima diffractometer) employing a nickel-filtered Cu-K α radiation. Sample morphology and structure details were characterized by transmission electron microscope (TEM, JEM-2100F). Surface area was measured by a Brunauer-Emmett-Teller (BET) analysis using a Tristar 3000 surface area analyzer. The X-ray photoelectron spectrum (XPS, Thermo Fisher Scientific ESCALab250) was also recorded in this experiment to confirm the surface component.

Results and discussion

X-ray diffraction (XRD) patterns of the as-prepared α -MnO₂ nanowires and α -MnO₂/Co₃O₄ hybrid are shown in Fig. 1a. All the peaks of the MnO₂ pattern can be indexed to a pure

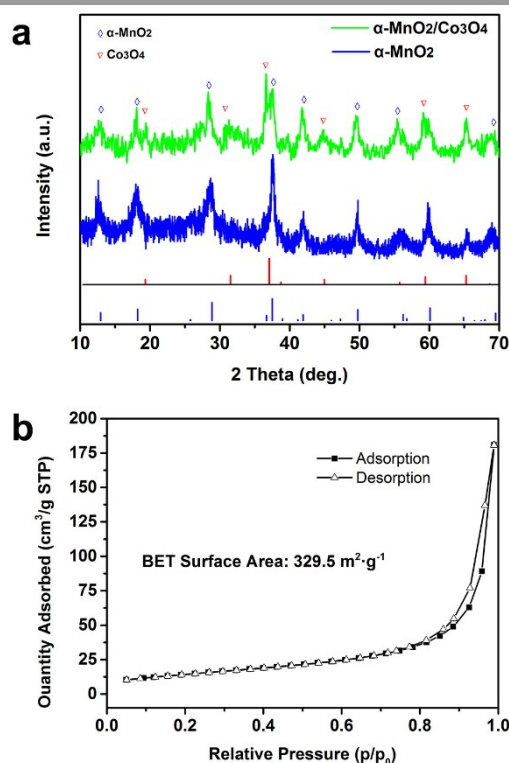


Fig. 1 XRD patterns of the prepared α -MnO₂ nanowires and α -MnO₂/Co₃O₄ hybrid (a), and typical N₂ gas adsorption-desorption isotherm of the α -MnO₂/Co₃O₄ hybrid.

tetragonal phase [space group: $I4/m(87)$] of $\alpha\text{-MnO}_2$ (JCPDS 44-0141). For $\alpha\text{-MnO}_2/\text{Co}_3\text{O}_4$ hybrid, the diffraction peaks at 19° , 31.3° , 36.9° , 44.8° , 59.4° , 65.2° can be indexed to (111), (220), (311), (222), (400), (422), (511) and (440) planes of Co_3O_4 , respectively. Fig. 1b is the N_2 adsorption/desorption curves, the Brunauer-Emmett-Teller (BET) surface area of the as-prepared sample is estimated to be about $329.5\text{ m}^2\cdot\text{g}^{-1}$, similar to the pure $\alpha\text{-MnO}_2$ ($325.4\text{ m}^2\cdot\text{g}^{-1}$), which is higher than most of the metal oxides catalysts used in Li-O_2 batteries up to date.^{18, 20} This kind of high specific surface area character could be benefit to the deposition of the discharge products.

The morphologies of as prepared $\alpha\text{-MnO}_2$ and $\alpha\text{-MnO}_2/\text{Co}_3\text{O}_4$ hybrid were examined using a transmission electron microscopy (TEM). As shown in Fig. 2a and b, the $\alpha\text{-MnO}_2$ samples show nanowire morphology with diameter 20-50 nm and length ranging between 5 and 10 μm . Fig. 2c, d shows that the Co_3O_4 nanoparticles with average size of 4-8 nm homogeneously coating on the surface of $\alpha\text{-MnO}_2$ nanowire. Fig. 2e shows a high-resolution TEM image of $\alpha\text{-MnO}_2/\text{Co}_3\text{O}_4$ hybrid and indicates clearly the (200) facet of $\alpha\text{-MnO}_2$ and the (220) facet of spinel Co_3O_4 .

By growing Co_3O_4 nanoparticles on the MnO_2 nanowires, we have synthesized a hybrid catalyst with excellent bi-functional activity for ORR and OER in Li-O_2 batteries. Typical cyclic voltammetry curves of the $\alpha\text{-MnO}_2/\text{Co}_3\text{O}_4$ and $\alpha\text{-MnO}_2+\text{Co}_3\text{O}_4$ at a scan rate of 0.2 mV s^{-1} between 2.0 and 4.3 V is shown in Fig. S2. The obviously higher ORR onset potential indicates the higher catalytic activity of $\alpha\text{-MnO}_2/\text{Co}_3\text{O}_4$. In addition, both the cathodic and anodic reactions of $\alpha\text{-MnO}_2/\text{Co}_3\text{O}_4$ are more pronounced than those of the $\alpha\text{-MnO}_2+\text{Co}_3\text{O}_4$ electrode. The

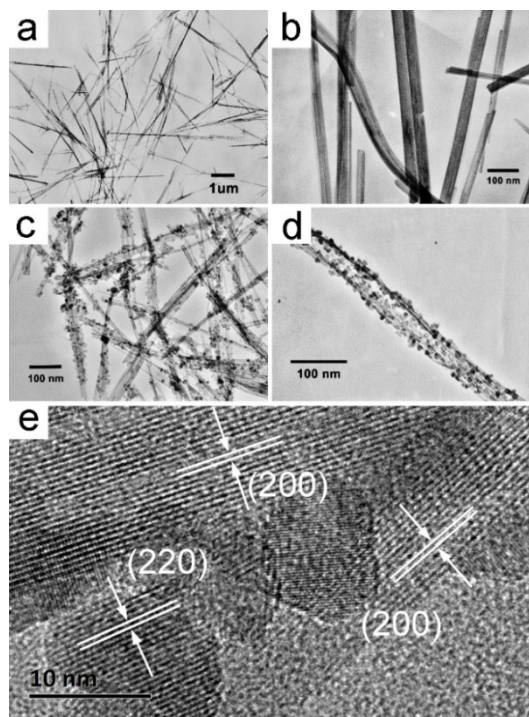


Fig. 2 TEM images of (a), (b) $\alpha\text{-MnO}_2$ and (c), (d) $\alpha\text{-MnO}_2/\text{Co}_3\text{O}_4$ hybrid; HRTEM image of the interface between MnO_2 nanotube and Co_3O_4 nanocrystals (e).

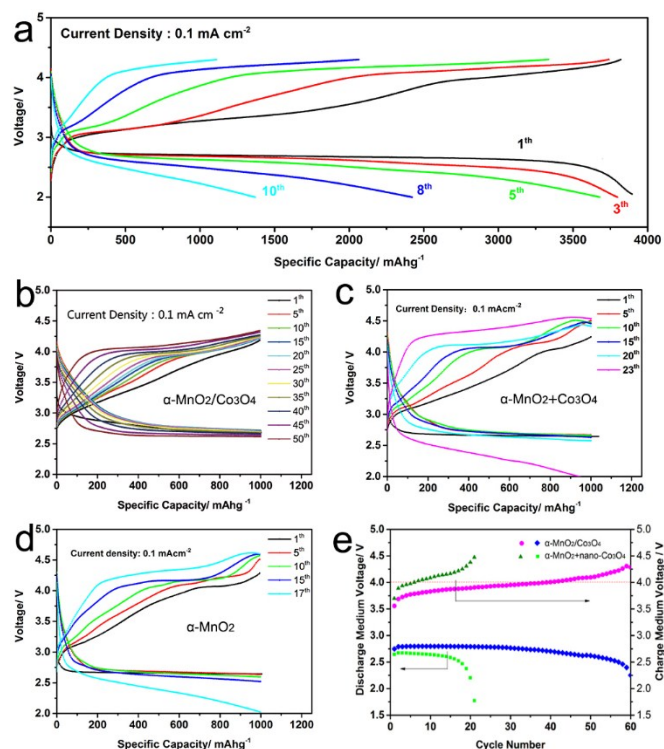


Fig. 3 Discharging and charging profiles of cell based on $\alpha\text{-MnO}_2/\text{Co}_3\text{O}_4$ (a), MnO_2 mixed with nano- Co_3O_4 (b) and pure $\alpha\text{-MnO}_2$ (c); the variation of discharge and charge medium voltage with the cycle number (d).

electrochemical performance of the cathodes of Li-O_2 cells was evaluated through a galvanodynamic method. The discharging and charging profiles of the $\alpha\text{-MnO}_2/\text{Co}_3\text{O}_4$ hybrid catalyst are shown in Fig. 3.

The discharge and charge measurement is carried out at $0.1\text{ mA}\cdot\text{cm}^{-2}$ in the voltage range of 2.0-4.2 V at room temperature. The discharge/charge voltage profiles are shown in Fig. 3a. The first specific capacity of the $\alpha\text{-MnO}_2/\text{Co}_3\text{O}_4$ hybrid electrode is $3900\text{ mAh}\cdot\text{g}^{-1}$ and capacity remain $1360\text{ mAh}\cdot\text{g}^{-1}$ after 10th cycle which shows good capacity retention. The initial charge-discharge profiles of $\alpha\text{-MnO}_2/\text{Co}_3\text{O}_4$ and comparative samples are shown in Fig. S1. We can find that the discharge/charge overpotential is efficiently reduced due to its good catalytic performance. The effect of $\alpha\text{-MnO}_2/\text{Co}_3\text{O}_4$ hybrid catalysts on the cycling performance of Li-O_2 batteries has been further tested with controlled depth of charge and discharge. The cell showed excellent cycling performance over 60 cycles with the specific capacity maintained $1000\text{ mAh}\cdot\text{g}^{-1}$ at the current density of $0.1\text{ mA}\cdot\text{cm}^{-2}$, much longer than those of MnO_2 (17 cycles) and mechanical mixture of MnO_2 and Co_3O_4 (23 cycles). As shown in the charge and discharge voltage curve (Fig. 3c), the discharge medium voltage was above 2.80 V, and the charge medium voltage below 3.90 V within 20 cycles, which obviously shows that the prepared $\alpha\text{-MnO}_2/\text{Co}_3\text{O}_4$ catalysts own a high catalytic performance both in OER and ORR. For comparison, mechanically mixed catalysts: $\alpha\text{-MnO}_2$ nanowire and Co_3O_4 nanoparticles ($\alpha\text{-MnO}_2+\text{nano-Co}_3\text{O}_4$) as well as the pure $\alpha\text{-MnO}_2$ were also investigated in Li-O_2 batteries (Fig. 3b, c). The discharge curves have the dramatically decreased after the 25th and 17th cycle for $\alpha\text{-MnO}_2+\text{nano-Co}_3\text{O}_4$ and pure $\alpha\text{-MnO}_2$

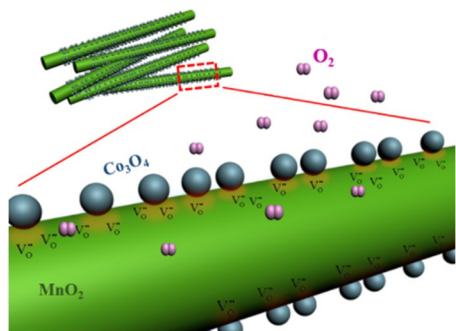


Fig. 4 Schematic diagram represents the oxygen vacancies generated on the surface of the MnO₂.

respectively. As displayed in Fig. 3c, the charge and discharge overpotential of α -MnO₂+Co₃O₄ mixture are obviously higher than that of the α -MnO₂/Co₃O₄ hybrid. To be specific, the discharge medium voltage of the hybrid was 0.2 V higher than α -MnO₂+nano-Co₃O₄ and 0.3 V lower for charge voltage.

The above results demonstrated that the α -MnO₂/Co₃O₄ hybrid electrode has a superior reversibility and a high performance towards both OER and ORR. The increased cycling performance may attribute to its high specific surface area which can supply numerous catalytic active sites and be beneficial for the efficient diffusion of both Li ion and oxygen. The good catalytic activity of the α -MnO₂/Co₃O₄ hybrid nanomaterials for the OER and ORR may also be attributed to the synergistic effect and the interfacial effect between the α -MnO₂ nanowire and the Co₃O₄ nanoparticles.

In order to characterize the interaction of the hybrid, Fourier Transform infrared spectroscopy (FTIR) and X-ray photoelectron spectra (XPS) both were further used. Fig. 5a shows the local magnified XRD patterns, which reveals a small shift in the peak position of the α -MnO₂/Co₃O₄ hybrid. This is due to the variation in lattice constants, which indicates that Co has entered into MnO₂ structure.³¹ Fig. 5b shows the FTIR spectra of α -MnO₂/Co₃O₄ hybrid compared with the mixture phase.

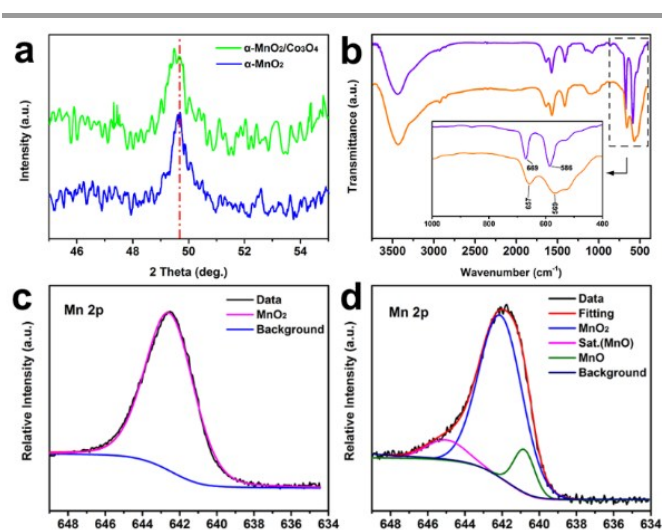
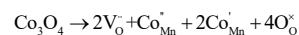


Fig. 5 Magnified XRD patterns of α -MnO₂ and α -MnO₂/Co₃O₄ (a), FTIR spectra of α -MnO₂+Co₃O₄ mixture and α -MnO₂/Co₃O₄ hybrid (b). XPS spectra of Mn 2p core-level recorded from the surface of α -MnO₂ (c) and α -MnO₂/Co₃O₄ hybrid (d).

Absorption peaks at the range of 400-1000 cm⁻¹ mainly correspond to the vibrations of Co-O and Mn-O bonds.^{32, 33} The XRD spectra of α -MnO₂/Co₃O₄ hybrid show identical peaks of MnO₂ and Co₃O₄, but slightly shift in the peak position, due to the disturbances generated with the interaction between cobalt and manganese ion.³⁴ To make a further validation, the XPS spectra was used to provide additional information about the α -MnO₂/Co₃O₄ hybrid surface. Fig. 5c, d illustrates the Mn 2p XPS spectra acquired from pure α -MnO₂ and α -MnO₂/Co₃O₄ specimens respectively with the Mn 2p_{3/2} peak position remaining nearly stationary at ~ 642.2eV. Deconvolution of the Mn 2p spectrum of Fig. 5d, revealed two components of the principal 2p_{3/2} line, namely: the peak at 642.1 eV and the another one at 640.8 eV, which correspond to Mn (IV), Mn (II) respectively. More information is available from the Mn 2p satellite feature. As is known that Mn exhibits satellite features shifted from the main 2p peak to higher binding energy by about 5 eV for MnO.³⁵ The satellite feature noticeable on the higher-binding-energy side of the Mn 2p_{3/2} near 645.0 eV originates from the charge transfer between outer electron shell of ligand and an unfilled 3d shell of Mn during creation of core-hole in the photoelectron process.³⁶⁻³⁸ These are all consistent with the presence of Mn (II), which would originate from some of the MnO₂ on the surface reduced during the hydrothermal treatments.

According to above analysis, the coated Co₃O₄ nanoparticles are not just in the physical contact with MnO₂, the cobalt ions can dope into MnO₂ lattice during the hydrothermal treatments. Through the interaction between MnO₂ and Co₃O₄, more oxygen vacancies would be generated on the surface of the MnO₂ nanowires.

The defect reaction for formation of oxygen vacancy can be described as follows:



Previous work has shown that the presence of oxygen vacancies at the surface of MnO₂ can enhance its catalytic activity for ORR.^{29, 39, 40} Though the catalytic mechanism in Li-O₂ batteries is unclear, it was shown that oxygen vacancies on the surface of metal oxides played a significant effect on electrocatalytic processes of both ORR and OER in Li-air batteries.⁴¹ Theoretical calculations and experimental analysis indicate that the strong chemical bond between metal and adsorbed oxygen on oxygen vacancy site would cause the elongation of O-O bond, which results in the furtherance of the activation and partial dissociation of O-O bond.^{39, 42} Tomsett also reported that the presence of oxygen vacancy at MnO₂ surface enhances its catalytic activity in ORR.⁴³ Therefore, the presence of surface oxygen vacancy is beneficial and imperative to the chemical reactions because it can bind the O₂ more strongly and can also accelerate their dissociation. Another reason may contribute to the catalytic activity of both MnO₂ and Co₃O₄. There are two kinds of surface sites in the α -MnO₂/Co₃O₄ system. Both of them can contribute to the catalytic effect towards ORR and OER. The surface synergistic effect also plays an important role in the catalytic reaction in Li-O₂ batteries. Fig. S3 is the SEM images of the two cathodes after discharge. Due

to the high catalytic activity, the discharge products mainly deposit on the surface of $\alpha\text{-MnO}_2/\text{Co}_3\text{O}_4$ cathode. In contrast, it disorderly aggregated on the $\alpha\text{-MnO}_2+\text{Co}_3\text{O}_4$ cathode. Because of the uniform growth of the discharge products on the surface of $\alpha\text{-MnO}_2/\text{Co}_3\text{O}_4$ hybrid, the discharge products could be easier and more completely decomposed during charge process, resulting in less side-reaction associated with carbon and electrolyte. That is why the cycle performance of the $\alpha\text{-MnO}_2/\text{Co}_3\text{O}_4$ hybrid cathode is stabler.

Finally, we also used X-ray photoelectron spectra to character the discharge products after charge and discharge processes. As shown in Fig. 6, the Li 1s and O 1s XPS spectra were collected and fitted. We could clearly see that the peaks at 532 eV⁴⁴ in O 1s XPS spectrum (Fig. 6a) and 54.8 eV⁴⁵ in Li 1s XPS spectrum (Fig. 6b) correspond to Li_2O_2 , indicating the formation of Li_2O_2 during discharge process. And these peaks disappear at the end of charge process, which reveals that the main product's reversible formation and decomposition. Obviously, Li_2CO_3 and other by-products also formed during the cycling process, which could be the main reason for the decay of the Li-O₂ batteries. The main reason would be due to the decomposition of the carbon and electrolyte. It has been reported that carbon is unstable above 3.5 V at the presence of Li_2O_2 .⁴⁶ The decomposition of the electrolytes at a high voltage range has also been suggested as a possible cause of the capacity loss upon cycling.

Conclusions

In summary, nanoscale $\alpha\text{-MnO}_2/\text{Co}_3\text{O}_4$ hybrid catalyst for Li-O₂ batteries was synthesized by two steps hydrothermal method. The hybrid catalyst exhibited excellent OER and ORR activities in Li-O₂ batteries. The causation may be possible because of the oxygen vacancies produced on the surface of the MnO_2 nanowire, and more active sites produced on the MnO_2 surface. It may improve the catalytic reactions of the OER and ORR. The overpotential of the cell was significantly reduced and the cycling performance is very stable. We believe that hybrids based on MnO_2 and Co_3O_4 nanoscale catalysts which are low cost and efficient will be promising electrocatalysts for enhancing the sluggish kinetics of ORR and OER in Li-O₂ batteries.

Acknowledgements

We highly acknowledge Prof. B. V. R. Chowdari (National University of Singapore) for his useful discussions. This experimental work of this study was supported by the Natural Science Foundation of China (NSFC, Project No.51432010, No.51272267 and No.51373195).

Notes and references

1. T. Ogasawara, A. Débart, M. Holzapfel, P. Novák and P. G. Bruce, *J. Am. Chem. Soc.*, 2006, **128**, 1390-1393.
2. G. Girishkumar, B. McCloskey, A. C. Luntz, S. Swanson and W. Wilcke, *J. Phys. Chem. Lett.*, 2010, **1**, 2193-2203.
3. J. Read, K. Mutolo, M. Ervin, W. Behl, J. Wolfenstine, A. Driedger and D. Foster, *J. Electrochem. Soc.*, 2003, **150**, A1351.
4. J. Xiao, D. H. Wang, W. Xu, D. Y. Wang, R. E. Williford, J. Liu and J. G. Zhang, *J. Electrochem. Soc.*, 2010, **157**, A487-A492.
5. K. Abraham and Z. Jiang, *J. Electrochem. Soc.*, 1996, **143**, 1-5.
6. Z. L. Wang, D. Xu, J. J. Xu and X. B. Zhang, *Chem. Soc. Rev.*, 2014, **43**, 7746-7786.
7. A. Debart, J. Bao, G. Armstrong and P. G. Bruce, *J. Power Sources*, 2007, **174**, 1177-1182.
8. J. Jung, K. Song, D. R. Bae, S. W. Lee, G. Lee and Y. M. Kang, *Nanoscale*, 2013, **5**, 11845-11849.
9. W. Y. Zhang, J. X. Zhu, H. X. Ang, Y. Zeng, N. Xiao, Y. B. Gao, W. L. Liu, H. H. Hng and Q. Y. Yan, *Nanoscale*, 2013, **5**, 9651-9658.
10. Y.-C. Lu, Z. Xu, H. A. Gasteiger, S. Chen, K. Hamad-Schifferli and Y. Shao-Horn, *J. Am. Chem. Soc.*, 2010, **132**, 12170-12171.
11. J. L. Shui, N. K. Karan, M. Balasubramanian, S. Y. Li and D. J. Liu, *J. Am. Chem. Soc.*, 2012, **134**, 16654-16661.
12. F. Wang, C. S. Liang, D. L. Xu, H. Q. Cao, H. Y. Sun and Z. K. Luo, *Journal of Inorganic Materials*, 2012, **27**, 1233-1242.
13. J. J. Xu, Z. L. Wang, D. Xu, L. L. Zhang and X. B. Zhang, *Nat. Commun.*, 2013, **4**, 2438.
14. J. J. Xu, D. Xu, Z. L. Wang, H. G. Wang, L. L. Zhang and X. B. Zhang, *Angew. Chem. Int. Edit.*, 2013, **52**, 3887-3890.
15. Q. C. Liu, J. J. Xu, D. Xu and X. B. Zhang, *Nat. Commun.*, 2015, **6**, 8.
16. L. Jin, L. P. Xu, C. Morein, C. H. Chen, M. Lai, S. Dharmarathna, A. Doble and S. L. Suib, *Adv. Funct. Mater.*, 2010, **20**, 3373-3382.
17. J. X. Li, N. Wang, Y. Zhao, Y. H. Ding and L. H. Guan, *Electrochem. Commun.*, 2011, **13**, 698-700.
18. Y. Cao, Z. Wei, J. He, J. Zang, Q. Zhang, M. Zheng and Q. Dong, *Energ. Environ. Sci.*, 2012, **5**, 9765-9768.
19. K. Song, J. Jung, Y. U. Heo, Y. C. Lee, K. Cho and Y. M. Kang, *PCCP*, 2013, **15**, 20075-20079.
20. A. Debart, A. J. Paterson, J. Bao and P. G. Bruce, *Angew. Chem. Int. Edit.*, 2008, **47**, 4521-4524.
21. E. M. Benbow, S. P. Kelly, L. Zhao, J. W. Reutenauer and S. L. Suib, *The Journal of Physical Chemistry C*, 2011, **115**, 22009-22017.
22. Y. M. Cui, Z. Y. Wen and Y. Liu, *Energ. Environ. Sci.*, 2011, **4**, 4727-4734.
23. Y. G. Li, B. Tan and Y. Y. Wu, *Nano Lett.*, 2008, **8**, 265-270.
24. W. Yang, J. Salim, C. Ma, Z. H. Ma, C. W. Sun, J. Q. Li, L. Q. Chen and Y. Kim, *Electrochem. Commun.*, 2013, **28**, 13-16.
25. H. Xia, M. O. Lai and L. Lu, *J. Mater. Chem.*, 2010, **20**, 6896-6902.
26. C. S. Park, J. H. Kim and Y. J. Park, *J. Electroceram.*, 2013, **31**, 224-230.
27. A. K. Thapa and T. Ishihara, *J. Power Sources*, 2011, **196**, 7016-7020.
28. G. Y. Zhao, J. X. Lv, Z. M. Xu, L. Zhang and K. N. Sun, *J. Power Sources*, 2014, **248**, 1270-1274.
29. D. A. Tompsett, S. C. Parker and M. S. Islam, *J. Mater. Chem. A*, 2014, **2**, 15509-15518.
30. X. Wang and Y. D. Li, *J. Am. Chem. Soc.*, 2002, **124**, 2880-2881.

31. A. M. A. Hashem, H. A. Mohamed, A. Bahloul, A. E. Eid and C. M. Julien, *Ionics*, 2008, **14**, 7-14.
32. C. M. Julien, M. Massot and C. Poinignon, *Spectrochimica Acta Part A: Molecular and Biomolecular Spectroscopy*, 2004, **60**, 689-700.
33. J. Jiang and L. Li, *Mater. Lett.*, 2007, **61**, 4894-4896.
34. A. Hashem, H. Mohamed, A. Bahloul, A. Eid and C. Julien, *Ionics*, 2008, **14**, 7-14.
35. V. Di Castro and G. Polzonetti, *J. Electron. Spectrosc. Relat. Phenom.*, 1989, **48**, 117-123.
36. M. Oku, K. Wagatsuma and T. Konishi, *J. Electron. Spectrosc. Relat. Phenom.*, 1999, **98-99**, 277-285.
37. R. J. Iwanowski, M. H. Heinonen, W. Paszkowicz, R. Minikae, T. Story and B. Witkowska, *Appl. Surf. Sci.*, 2006, **252**, 3632-3641.
38. S.-P. Jeng, R. J. Lad and V. E. Henrich, *Physical Review B*, 1991, **43**, 11971.
39. F. Cheng, T. Zhang, Y. Zhang, J. Du, X. Han and J. Chen, *Angew. Chem. Int. Ed.*, 2013, **52**, 2474-2477.
40. D. M. Robinson, Y. B. Go, M. Mui, G. Gardner, Z. Zhang, D. Mastrogiovanni, E. Garfunkel, J. Li, M. Greenblatt and G. C. Dismukes, *J. Am. Chem. Soc.*, 2013, **135**, 3494-3501.
41. S. H. Oh, R. Black, E. Pomerantseva, J.-H. Lee and L. F. Nazar, *Nat. Chem.*, 2012, **4**, 1004-1010.
42. F. Y. Cheng, J. A. Shen, B. Peng, Y. D. Pan, Z. L. Tao and J. Chen, *Nat. Chem.*, 2011, **3**, 79-84.
43. D. A. Tompsett, S. C. Parker and M. S. Islam, *J. Am. Chem. Soc.*, 2014, **136**, 1418-1426.
44. J. Lu, Y. Qin, P. Du, X. Y. Luo, T. P. Wu, Y. Ren, J. G. Wen, D. J. Miller, J. T. Miller and K. Amine, *Rsc Adv.*, 2013, **3**, 8276-8285.
45. Y. Lei, J. Lu, X. Luo, T. Wu, P. Du, X. Zhang, Y. Ren, J. Wen, D. J. Miller, J. T. Miller, Y.-K. Sun, J. W. Elam and K. Amine, *Nano Lett.*, 2013, **13**, 4182-4189.
46. M. M. O. Thotiyl, S. A. Freunberger, Z. Q. Peng and P. G. Bruce, *J. Am. Chem. Soc.*, 2013, **135**, 494-500.